Exome sequencing and metabolomic analysis of a chronic kidney disease and hearing loss patient family revealed RMND1 mutation induced sphingolipid metabolism defects

Nagwa E.A. Gaboon [a,b,1], Babajan Banaganapalli [a,c,1], Khalidah Nasser [c,d], Mohammed Razeeth [e], Mosab S. Alsaedi [a], Omran M. Rashidi [c], Lereen S. Abdelwehab [f], Turki Saad Alahmadi [g], Osama Y. Safdar [h], Jilani Shaik [i], Hani M.Z. Choudhry [e], Huda Husain Al-numan [c,j], Mohammad Imran Khan [e,*], Jumana Y. Al-Aama [a,c], Ramu Elango [a,c,*], Noor A. Shaik [a,c,*]

[a] Department of Genetic Medicine, Faculty of Medicine, King Abdulaziz University, Jeddah, Saudi Arabia
[b] Medical Genetics Centre, Faculty of Medicine, Ain-Shams University, Cairo, Egypt
[c] Princess Al-Jawhara Al-Brahim Center of Excellence in Research of Hereditary Disorders, King Abdulaziz University, Jeddah, Saudi Arabia
[d] Department of Medical Laboratory Technology, Faculty of Applied Medical Sciences, King Abdulaziz University, Jeddah, Saudi Arabia
[e] Department of Biochemistry, King Abdulaziz University, Jeddah, Saudi Arabia
[f] Faculty of Medicine, Ain Shams University, Cairo, Egypt
[g] Department of Pediatrics, Faculty of Medicine, King Abdulaziz University, Jeddah, Saudi Arabia
[h] Pediatric Nephrology Center of Excellence, King Abdulaziz University, Jeddah, Saudi Arabia
[i] Genome Research Chair, College of Science, King Saud University, Saudi Arabia
[j] Department of Biological Sciences, Faculty of Science, King Abdulaziz University, Jeddah, Saudi Arabia

ARTICLE INFO

ABSTRACT

Mitochondrial disorders (MIDs) shows overlapping clinical presentations owing to the genetic and metabolic defects of mitochondria. However, specific relationship between inherited mutations in nuclear encoded mitochondrial proteins and their functional impacts in terms of metabolic defects in patients is not yet well explored. Therefore, using high throughput whole exome sequencing (WES), we screened a chronic kidney disease (CKD) and sensorineural hearing loss (SNHL) patient, and her family members to ascertain the mode of inheritance of the mutation, and healthy population controls to establish its rare frequency. The impact of mutation on biophysical characteristics of the protein was further studied by mapping it in 3D structure. Furthermore, LC-MS tandem mass spectrophotometry based untargeted metabolomic profiling was done to study the fluctuations in plasma metabolites relevant to disease causative mutations and kidney damage. We identified a very rare homozygous c.631G > A (p.Val211Met) pathogenic mutation in RMND1 gene in the proband, which is inherited in an autosomal recessive fashion. This gene is involved in the mitochondrial translational pathways and contribute in mitochondrial energy metabolism. The p.Val211Met mutation is found to disturb the structural orientation (RMSD is −2.95 Å) and stability (ΔΔG is −0.552 Kcal/mol) of the RMND1 protein. Plasma metabolomics analysis revealed the aberrant accumulation of metabolites connected to lipid and amino acid metabolism

Production and hosting by Elsevier

pathways. Of these metabolites, pathway networking has discovered ceramide, a metabolite of sphingolipids, which plays a role in different signaling cascades including mitochondrial membrane biosynthesis, is highly elevated in this patient. This study suggests that genetic defects in *RMND1* gene alters the mitochondrial energy metabolism leading to the accumulation of ceramide, and subsequently promote dysregulated apoptosis and tissue necrosis in kidneys.

1. Introduction

Mitochondrial disorders (MIDs) are known for their variable phenotypic expression and complex genetic basis that is commonly caused by molecular defects of mitochondrial respiratory chain pathways. It has been demonstrated that one-third of MIDs patients present defects related to oxidative phosphorylation pathway genes (Kemp et al., 2011). Major organ systems affected in MIDs are endocrine organs, kidneys, heart, ears, eyes, skeletal muscles, and central nervous system (Finsterer and Scorza, 2017). Majority of the MID patients manifest renal dysfunctions in the form of acute or chronic failure, renal cysts, renal tubular acidosis (RTA), nephrotic syndrome, Toni-Debré-Fanconi syndrome (TDFS), Bartter-like syndrome, tubulointerstitial nephritis (TIN), nephrocalcinosis, focal segmental glomerulosclerosis (FSGS), and benign or malignant neoplasms (Finsterer and Frank, 2016). However, renal involvement alone is not necessarily suggestive of MIDs. Its manifestation can either be as a dominant phenotype among the diverse clinical spectrum or as an additional-non-dominant phenotype (Finsterer and Scorza, 2017).

Different studies have successfully described a molecular basis of the disease diversified phenotypic spectrum using whole exome sequencing (WES) (Taylor et al., 2014; Ng et al., 2016; Casey et al., 2016). WES analysis facilitates rapid molecular diagnosis of clinically challenging cases and their family members by providing a quick and comprehensive information about known or novel mutations in candidate genes. One of the recently identified nuclear genes involved in mitochondrial respiratory chain deficiencies is *RMND1* (Required for Meiotic Nuclear Division protein 1) (Garcia-Diaz et al., 2012; Janer et al., 2012). It has been demonstrated that various novel and common recessive mutations in *RMND1* are associated with multiple phenotypes characterized by delayed maturation of vision, developmental delay, dilated cardiomyopathy, deafness and neurological defects (Gupta et al., 2016), renal tubular acidosis type 4 presented as hyponatraemia and hyperkalaemia and cystic/hypoplastic kidneys (Ng et al., 2016). Likewise, complex clinical spectrum of patients with *RMND1* mutations is emerging with infantile encephalomyopathy with lactic acidosis (Garcia-Diaz et al., 2012; Casey et al., 2016) to a less severe form of developmental delay, hypotonia, renal disease and congenital sensorineural deafness (Janer et al., 2015). Therefore, molecular screening of *RMND1* gene will help identify the inheritance mode of causative genetic mutations in patients with renal and or neurological defects.

MIDs have complex etiologies with underlying cross talk of inter and intra molecular signaling. Hence, metabolomic studies on these patients could provide a better understanding of the interconnectivity between genetic and molecular networks (Davies, 2018). Metabolomic profiling examines the metabolic changes in body fluids driven from cellular processes to understand the onset and pathogenesis of disease phenotype (Abbiss et al., 2019). Metabolomics analyzes metabolites by either targeted or untargeted approaches. The untargeted approach involves hypothesis free surveying of hundreds of thousands of small molecule metabolites for discovering novel mechanisms or pathways, whereas the targeted one refers to measuring predefined sets of metabolites, typically focusing on a few pathways of interest (Kalim and Rhee, 2017). The specific relationship between inherited mutations in mitochondrial proteins and their functional impacts in terms of metabolic defects in chronic kidney disease (CKD) is not yet well characterized. Therefore, we expect that WES based molecular diagnosis of MIDs will provide some hints in discovering either novel or known defective cellular metabolic networks, which would eventually aid in the etiology-based classifications of patient cohorts in future clinical studies.

By undertaking a multi-omics approach like WES, systems biology, and metabolomics, this study provides further insights about how inherited mutations in genes involved in normal functions of the mitochondria, perturbs the metabolome and causes complex disease phenotypes like CKD, neurological defects and hearing loss.

2. Materials and methods

2.1. Recruitment of patient and family members

This study has recruited 7 years old child presenting complex phenotypes including sensorineural hearing loss (SNHL), stage 3 CKD, and history of random seizures precipitated by crying for 30 s, followed by postictal drowsiness. The paternal and maternal uncles of the proband were reported to have similar clinical presentations of childhood onset of deafness and CKD followed by death before their 10th year of life. Born to the healthy consanguineous Arabian couple, this index proband was referred to genetic clinic from nephrology department for molecular diagnosis and subsequent genetic counselling. All the clinical details were revisited by the geneticist, and a multi-generation pedigree was drawn after interviewing both parents (Fig. 1). Before collection of 5 ml of blood samples, parental written consent was obtained after providing a detailed clarification about the nature of the study, the potential risks and benefits of the study outcomes for the patient and family members. This study received the ethical committee approval from King Abdulaziz University (KAU).

2.2. Molecular genetic tests

2.2.1. Genetic analysis

WES analysis was done for index case, and then prioritized variant in a candidate gene was validated by Sanger sequencing, and its mode of inheritance in the family was ascertained by Sanger sequencing method.

2.2.2. DNA isolation

The genomic DNA was isolated from circulating lymphocytes using QIAamp DNA blood kit according to the manufacturer's instructions (Qiagen, USA). Using NanoDrop ND-1000 UV–VIS spectrophotometer, DNA concentration, and purity were assessed. The quality of genomic DNA and the average molecular weight of each sample were assessed using agarose gel electrophoresis method.
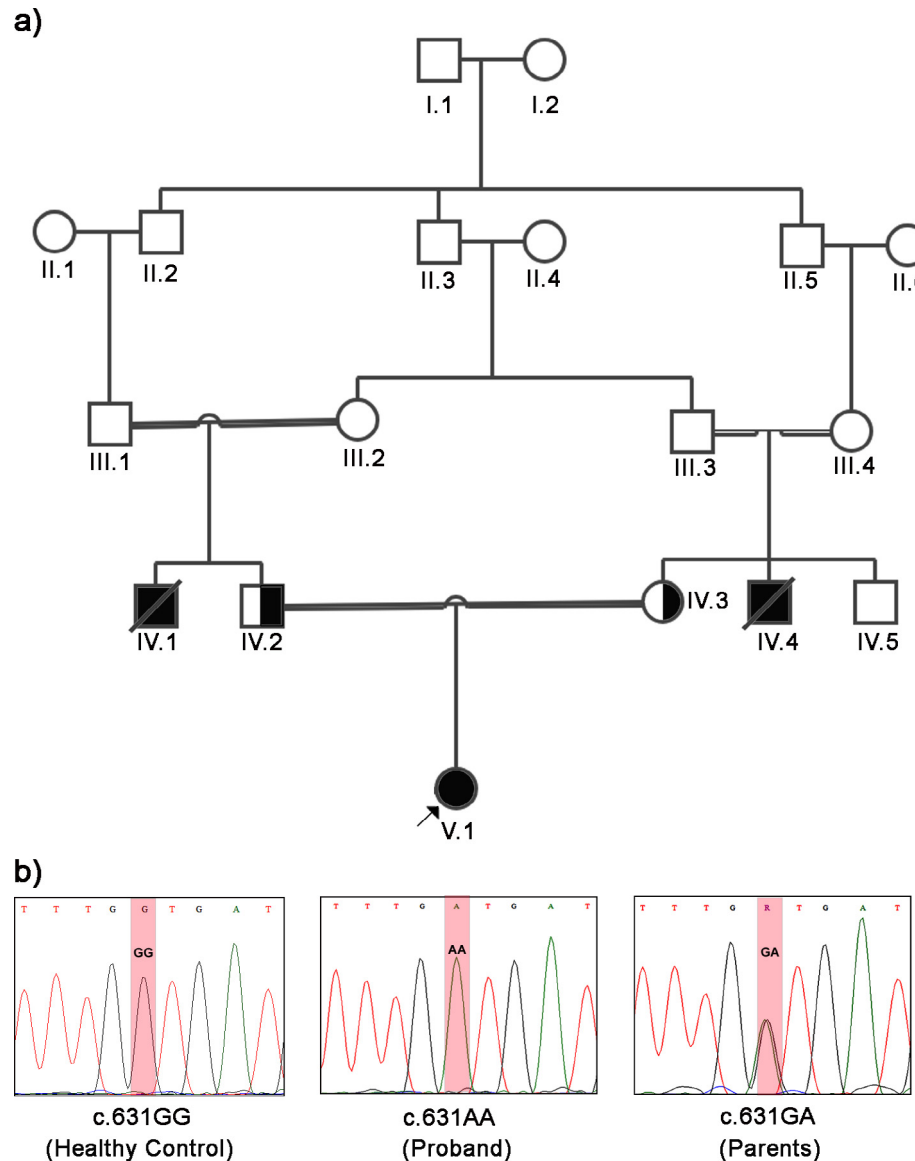
Fig. 1. (a) A multigeneration pedigree of a patient with chronic kidney disease and sensorineural hearing loss: IV.1 and IV.4 are deceased. IV.2 and IV.3 represents that the consanguineous couple carries the c.631G > A mutation of *RMND1* in heterozygous state. V.1 represents that CKD patient is homozygous to *c.631AA* pathogenic mutation of *RMND1*. (b) Sanger sequencing results: Sanger sequencing chromatogram of c.631G > A *RMND1* mutation seen in healthy control (GG), her parents (GA) and index case (AA).

2.2.3. Whole exome sequencing (WES)

The genomic DNA of 100 ng/μl was used for the whole exome-enriched library from the affected proband. All exonic regions of the protein encoded genes registered in CCDS and RefSeq databases were trapped using Agilent SureSelect capture kit (Agilent Technologies, USA). HiSeq2000 llumina platform was used to generate large scale short read sequencing. The sequencing reads were mapped against the human reference genome assembly (GRC38, NCBI) using BLAST (version 0.6.4d). GATK and SAM tools were used for base quality recalibration and variants calling such as SNPs and indels, respectively. The minimum coverage for variants calling was set at 30X. High quality Phred scoring of 30 was set for reads on both strands to be included as potential variants. The allele frequency of identified common variants (>1%) was ruled out as potential causative mutations based on dbSNP142, the Exome Aggregation Consortium (ExAC) databases, 1000 Genomes Pilot 1 datasets, Greater Middle East (GME) Variome Project and Saudi Human Genome Project (SHGP). Furthermore, we did whole exome sequencing of the 65 healthy Arab control volunteer samples and

used that data in filtering the potential disease linked rare allelic variants. The prediction of the functional effect of non-synonymous mutations was carried out using PolyPhen-2, the SIFT, and Mendelian Clinically Applicable Pathogenicity (M-CAP) tools (Al-Aama et al., 2017; Shaik and Banaganapalli, 2019).

2.2.4. Trio family screening for candidate mutations using targeted sequencing approach

Potential disease causative variant of *RMND1* gene identified in the proband was further screened in both unaffected parents (Fig. 1) using traditional dideoxynucleotide sequencing method. For target genomic enrichment, primers were custom-designed using open source software PRIMER3; (http://frodo.wi.mit.edu/) flanking the candidate variant alleles (Forward Primer: 5′-TCACC TAATGGGGTTTCTTTC-3′ & Reverse Primer: 5′-CCTTTCAGAGGCCT TAGTAG-3′). Gradient PCR was conducted to optimize the annealing temperature condition for primers (annealing temperature: 59 °C). Following this, 35 cycles of PCR amplifications were performed, and the success of the PCR was assessed using agarose

gel electrophoresis before target purification and cycle sequencing on ABI-Prism 3700 Genetic Analyzer. The rationale of this was to confirm the segregation of causative mutation in this family and to identify its mode of inheritance.

2.3. 3D structural assessment of RMND1 mutation

In this study, the 3D structure of the wild type *RMND1* protein was built *in-silico* as there is neither solved structure (crystal structure) nor homologous templates available in the database. Thus, we experimentally modeled the wild type and mutant *RMND1* protein structure and examined the structural stability and its dynamic behavior under physiological conditions, through *ab-initio* modeling technique using I-Tasser web tool. Following iterative template fragment approach, this webserver constructs full length 3D protein models of query proteins, on the basis of the structure templates available in protein database. The Input options provided to the I-Tasser website is *RMND1* amino acid sequence (retrieved from KEGG database KG: 55005) pasted in the search box in FASTA format. The output was the result of protein structure and its quality scores like confidence (C) score, root mean square deviation (RMSD) and template model (TM) scores (Al-Abbasi et al., 2018). The best predicted 3D protein model was energy minimized and later used to construct mutant version of *RMND1* protein by homology modelling approach. The 3D structures of both native and mutant *RMND1* proteins were examined by PyMol program for structural dissimilarities at the amino acid residue level. The stability analysis of mutant *RMND1* protein is estimated by Dynamut webserver (Rodrigues et al., 2018).

2.4. Plasma metabolomics analysis

We performed the plasma metabolomics of CKD index case and both parents. The basic steps of metabolomics are given below.

2.4.1. Metabolite extraction

Metabolites from patient plasma were extracted using a combination of Methanol: Acetonitrile: water ratio of 2:2:1 v/v with 100 μl plasma and 400 μl of ice-cold solvent added and vortexing (30 sec) followed by incubation at $-20\,^{\circ}C$ for one hour. The extracted metabolites were centrifuged (at 13,000 rpm/15 min/4 °C). The resulting supernatant was dried using speed vacuum concentrator. The dried metabolites were resuspended in 100 μl of ACN: water (1:1, v/v), vortexed (for 10 min) and spin (at 13000 rpm/15 min/4°C) to remove debris. The extracts were taken for LC-MS/MS.

2.4.2. HPLC workflow

A total of 10 uL of the sample was injected into HPLC. The column used is Hypersail gold (150 mm × 4.6 mm, 5 μm). The mobile phase buffer A (0.1% Formic acid) and buffer B (99.9% ACN formic acid (0.1%, v/v)) were used in linear gradient program, where the component of solution was changed from 5% B to 100% B over 90 min at a flow rate of 0.25 ml/min; 95% A from 5% to 30% over 72 min, 30% to 100% over 10 min, and kept at 100% for 5 min with flow rate of 200 ml/min and column temperature was kept constant at 30 °C.

2.4.3. Mass spectrometry parameter

LTQ XL™ linear ion trap instrument (Thermo Fisher Scientific) was used. Full scan scope was chosen from 100 to 1000 m/z. The capillary voltage was fixed at 4.0 V, and -3.0 kV was set as a spray voltage and the temperature at 270 °C. Sheath gas nitrogen with a flow rate of 40 arbitrary units and Helium gas as buffer gas is used. Data processing (RAW file) was carried out using Xcalibur software.

2.4.4. Data processing

Data processing was performed using XCMS, which processed the raw data and performed multiple feature recognition (peak intensity, molecular weight, atom nature), correcting the retention time and alignment. The default settings used in XCMS are as follows: centWave settings for feature detection (Δ m/z = 30 ppm, minimum peak width = 10 s and maximum peak width = 120 s) and mzwid = 0.25, minfrac = 0.5, and bw = 10 for chromatogram alignment. After careful evaluation, retention time alignment was not required. Isotopic peaks and adducts were detected using CAMERA, a Bioconductor package. The precursor was then matched to METLIN at 20 ppm accuracy.

2.4.5. Statistical analysis

Statistical analysis was performed on metabolomic data using Metaboanalyst online tool (https://www.metaboanalyst.ca/). Trios spectral peak intensity data in triplicate samples were initially filtered using option inter-quantile range (IQR), followed by data normalization (sample normalization by median, data transformation by gLog, data scaling by mean-centered and divided by the standard deviation of each variable). Univariate analysis by one-way analysis of variance (p-value false discovery rate [FDR] cutoff 0.05) and correlation analysis was performed on metabolomic data. The chemometric analysis was carried out by principal component analysis (PCA) to understand the probability of correlated metabolites into a set of values of linearly uncorrelated metabolites.

2.4.6. Metabolomics pathway analysis

The differentially enriched metabolites and corresponding metabolic pathways in the proband were identified by Metaboanalyst (https://www.metaboanalyst.ca/faces/home.xhtml) webserver following the standard methodology of metabolite set enrichment analysis basing on KEGG pathway database (https://www.genome.jp/kegg/pathway.html) as a reference. Pathway enrichment was determined by hypergeometric test and reported with an FDR-adjusted p-value.

3. Results

3.1. Clinical presentation

The patient *(V-1,* Fig. 1a*)* displayed normal early mental and motor development, with delayed speech. She came to medical attention at 2 years of age due to failure to respond to voices. The audiogram showed bilateral severe to profound SNHL (Fig. 2 a-c). At the age of 5 years, the proband was incidentally identified to have stage 3 CKD, confirmed via pelvic ultrasound that showed bilateral echogenic kidney, and blood renal function test results were also consistent with CKD. Her blood creatinine level was 149 μmol/L (normal range: 53–115 μmol/L), glomerular filtration rate (GFR): 28 ml/min (normal value is >90 ml/min), urea (BUN): 35.9 mmol/L (normal range: 2.5–6.4 mmol/L), bicarbonate (HCO3) 18 mmol/L, albumen: 37.2 g/l (normal range: 40.2–47.2 g/l). Her bone function profile showed elevated phosphate (phos): 1.88 mmol/l (normal range: 0.8–1.58 mmol/l), normal calcium levels (Ca): 2.25 (normal range: 1.12–2.52 mmol/l), and within normal range for alkaline phosphatase (ALPI): 184 U/L (normal range: 156–369 U/L), elevated parathyroid hormone (PTH): 24.1 Pmol/L (normal range: 1.18–8.43 Pmol/L), normal sodium, levels (Na): 143 mmol/L (normal range: 136–145 mmol/L), borderline low potassium levels (K): 3.4 mmol/L (normal range: 3.5–5.1 mmol/L). No history of oliguria/ polyuria, pneumonia, recurrent diarrhea, vomiting, or chronic intake of any medication. The index case presented with hypertelorism and depressed nasal bridge.
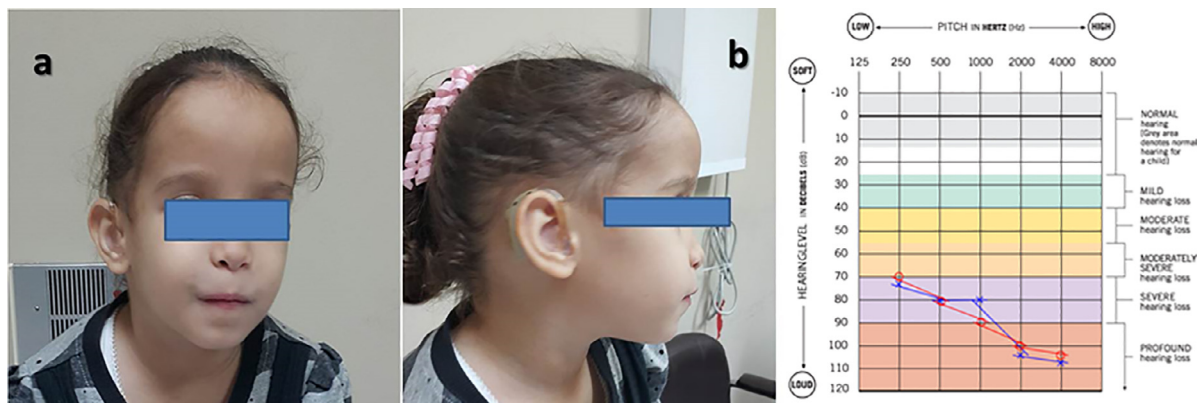
Fig. 2. (a) Affected index case photo frontal, (b) lateral views showing hearing aids, and (c) audio graphic evaluation.

SNHL was confirmed followed by wearing bilateral hearing aids (Fig. 2a–c). No characteristic odor was felt. On clinical assessment at the age of seven years, she had a stunted growth (her height was 100 cm at −4 SD), microcephaly (skull circumference was 49 cm, at −2SD) and was underweight (12.6 kg; <3rd percentile), BMI 12.6 (<5th centile). Her fundus examination, cardiac, and respiratory assessment was normal. The paternal uncle (IV-1, Fig. 1a) was severely affected and diagnosed to have deafness at 7 months of age, along with a history of recurrent seizures preceded by crying and stress. His renal function test was normal until the age of 6 years when he was diagnosed with CKD and deceased at the age of 7 years. Her maternal uncle (IV-4, Fig. 1a) was diagnosed with CKD and deafness during the investigation of recurrent attacks of vomiting at the age of 5 years and deceased at 7 years of age.

3.2. Molecular genetic analysis

3.2.1. Identification of presumptive pathogenic variant in the RMND1 gene

The exome consensus coding sequences were sequenced at an average depth (per base) of 80X, with more than 20X for ~89% targeted bases. By filtering the WES data, a novel rare missense pathogenic coding variant [NM_017909.3, c.631G > A, p. (Val211Met) located at 6:151754348 mapping to RMND1 gene was found to be present in the homozygous condition in the proband. The SIFT, PolyPhen-2, and M-CAP computational programs have designated the RMND1, c.631G > A variant as deleterious (score is 0.01), possibly damaging (score is 0.898) and possibly pathogenic (score is 0.031) respectively. This finding supports our suspicion that RMND1 genetic defects is central to chronic kidney disease in the proband.

3.2.2. Validation of family specific variant using Sanger-based sequencing method

The segregation of novel RMND1 variant (NM_017909.3, c.631G > A, p.Val211Met) in this family was validated in the family by using candidate gene sequencing approach (Fig. 1b). Both unaffected parents were heterozygous carriers (GA genotype) for the novel pathogenic variant, while the affected proband was homozygous for the mutant (AA genotype). Thus, the mode of inheritance for the variant was confirmed to be autosomal recessive. Sequencing trace files were compared with one control sample showing homozygous wild type alleles (GG genotype).

3.3. Structural analysis of RMND1 mutation

The RMND1 native protein structure predicted by I-Tasser webserver had the c score of −1.65, TM score of 0.35 ± 0.05, and an RMSD score of 12.2 ± 3.0 Å. These scores reflect the high quality of the predicted model and accurate folding of polypeptide chains in RMND1. The stereochemical check of full length RMND1 model showed that almost 98.3% of amino acid residues in both native and mutant forms of RMND1 protein are in the core region and 1.7% are in the non-core region suggesting the good stereochemical quality of the predicted structure. Superimposition of RMND1-3D structures (native and mutant) revealed the changes in volume and residue score of mutant Met211 (2.95 Å) residue compared to native Val211 residue of RMND1. The stability analysis of Met211 residue seems destabilizes RMND1 protein, as it could shift the Gibbs free energy values ($\Delta\Delta G$) in negative range (−0.552 Kcal/mol). The substitution of Met211 seems to destabilize the RMND1 protein by altering the hydrogen binding characteristics of amino acid residues from Leu191 to Leu202 and Lys423 to Phe449 (Fig. 3).

3.4. Metabolomic analysis

The initial XCMS analysis resulted in 231 mass to charge ratio (m/z) features in trios' sample. For identifying the significantly up and down regulated metabolites in trios, one-way ANOVA statistical test was conducted by fisher's LSD (Least significant difference) method ($p < 0.05$), (Fig. 4A), which finally resulted in identifying 151 most significant features between the patient and parents. PCA was performed to further compress the data set and make a visible pattern of overlapped metabolites among trios samples (Fig. 4B). Heatmap of metabolomic data showed the distribution of different plasma metabolites that were significantly different between parents and CKD patient (Fig. 4C). Despite the fold change differences, consistency in the overlapping feature was seen between patient and father's sample, with most metabolic compounds differentially regulated compared with both parents. These compounds are of diverse structures and functions, ranging from amino acids, lipids and nucleosides. This structural diversity supports the analytical capacity of untargeted metabolomics as a guiding tool for etiologic inquiry of kidney disease.

Pathway analysis with MetaboAnalyst 3.0 showed the involvement of multiple metabolites connected to exogenous and endogenous metabolism (e.g., lipid and amino acids metabolism, Fig. 5A) with pathway impact value of 0.01–0.5. Specifically, the metabolism of sphingolipids, which plays a very important role in signaling cascades for plasma membrane biosynthesis compounds such as ceramide, sphingosine, 3-Dehydrosphinganine, and galabiosylceramide (Fig. 5B). These metabolites showed the most elevated levels in the proband. Also, two other major lipid metabolic pathways markedly changed, as reflected in the alteration of bile acid and propanoate after sphingolipids (Table 1). Statistical analysis revealed that the elevated level of ceramide in the patient
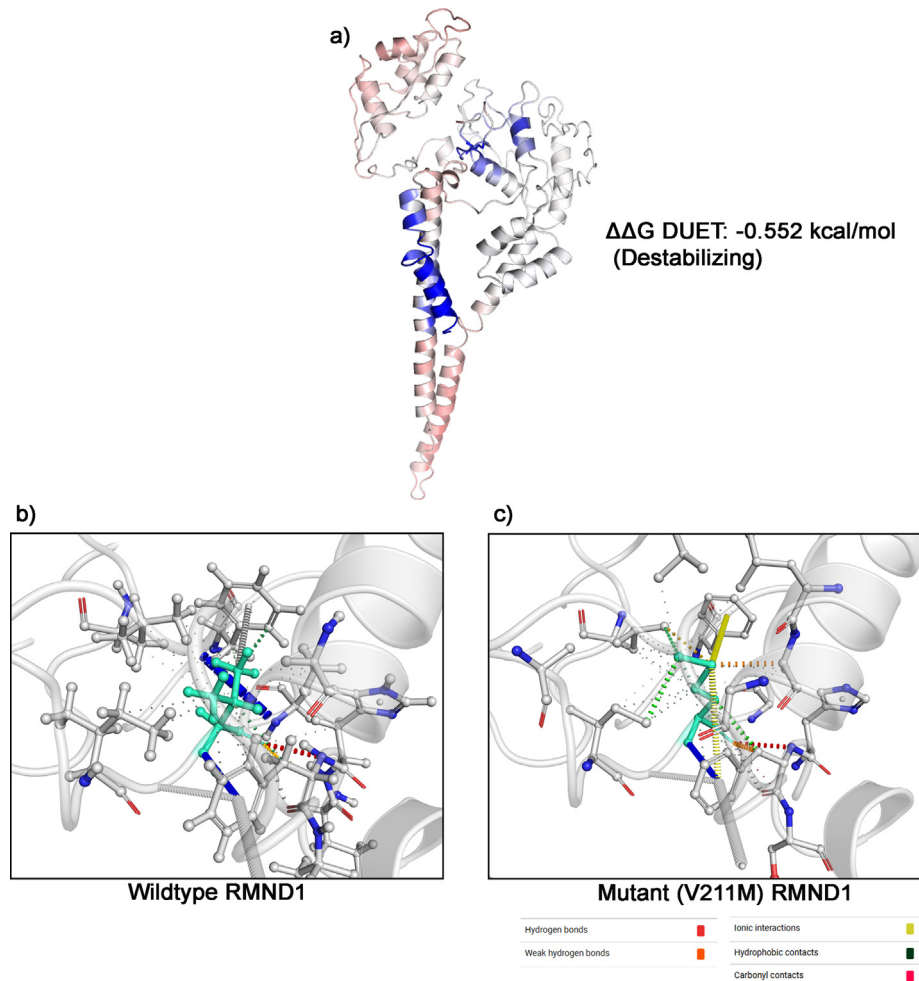
Fig. 3. The *RMND1* protein shows differences in stability (a) and hydrogen bonding characteristics in native (b) and mutant forms (c).

sample recorded is the most significant metabolite (p < 0.05) (Table 2).

To better assess the relationship between differentially expressed metabolites, *RMND1* gene, and other reported kidney disease genes, an in-depth pathway analysis was performed using STITTCH tools to construct the metabolite-protein interactions network. Various metabolites such as cholesterol, sphingomyelin, sphingosine, and phosphatidylethanolamine showed direct interactions with ceramide, which play a very important role in lipid metabolism (Fig. 6). Also, ceramide is enriched with networking with various key mitochondrial and apoptotic proteins such as CASP3, CASP9, and KDHS. The *RMND1* is not directly involved in the interaction with ceramide, but it is enriched along with CASP3 protein, which directly interacts with ceramide (Fig. 7).

4. Discussion

The *RMND1* protein is 449 amino acids long, and is involved in the mitochondrial translational pathway (Garcia-Diaz et al., 2012; Janer et al., 2012). Recent *in-vitro* studies demonstrated that knocked down cells of *RMND1* gene resulted in reduced mitochondrial protein synthesis and diminished mitochondrial complex activity (Garcia-Diaz et al., 2012). Likewise, (Janer et al., 2012; Janer et al., 2015) provided insights towards the requirement of *RMND1* protein in the mitochondrial translational network, handling of post mRNAs transcripts with their translation and

mitochondrial ribosome stability. Thus, *RMND1* recessive mutations lead to mitochondrial respiratory chain deficiencies and generalized defects in mitochondrial metabolism involving translational pathways (see Fig. 8).

The clinical manifestations of mitochondrial diseases includes congenital sensorineural deafness, hypotonia, lactic acidaemia, and multiple mitochondrial respiratory chain deficiencies. All of which were previously seen in other mitochondrial diseases with renal defects (Che et al., 2014). The genetic causes underlying the mixed phenotypes of the disease has been explained following the detection of homozygous splice site mutation in the *RMND1* gene (IVS2DS, G-A, +1) causative to COXPD11 (Combined Oxidative Phosphorylation Deficiency) patients belonging to a Saudi Arabian consanguineous family (Garcia-Diaz t al., 2012). Likewise, pathogenic homozygous mutations (R417Q; 614917.0002, (c.1349G > C (p.*450Serext*32)) and compound heterozygous mutations (ASN238SER & IVS3DS, G-T, +1) were detected in *RMND1* gene from affected girl with COXPD11, another 5 unrelated affected children of a consanguineous British Pakistani parents, and affected boy with COXPD11 respectively using WES (Janer et al., 2012, 2015). Cultured cells from patient fibroblast showed reduced ribosomal subunits of mitochondria and translational defects of mitochondrial proteins (Janer et al., 2015). These findings confirm the important role of *RMND1* protein in the mitochondrial translational network.

The disease is characterized by multisystem features involving lactic acidosis, respiratory insufficiency, profound deafness, foot
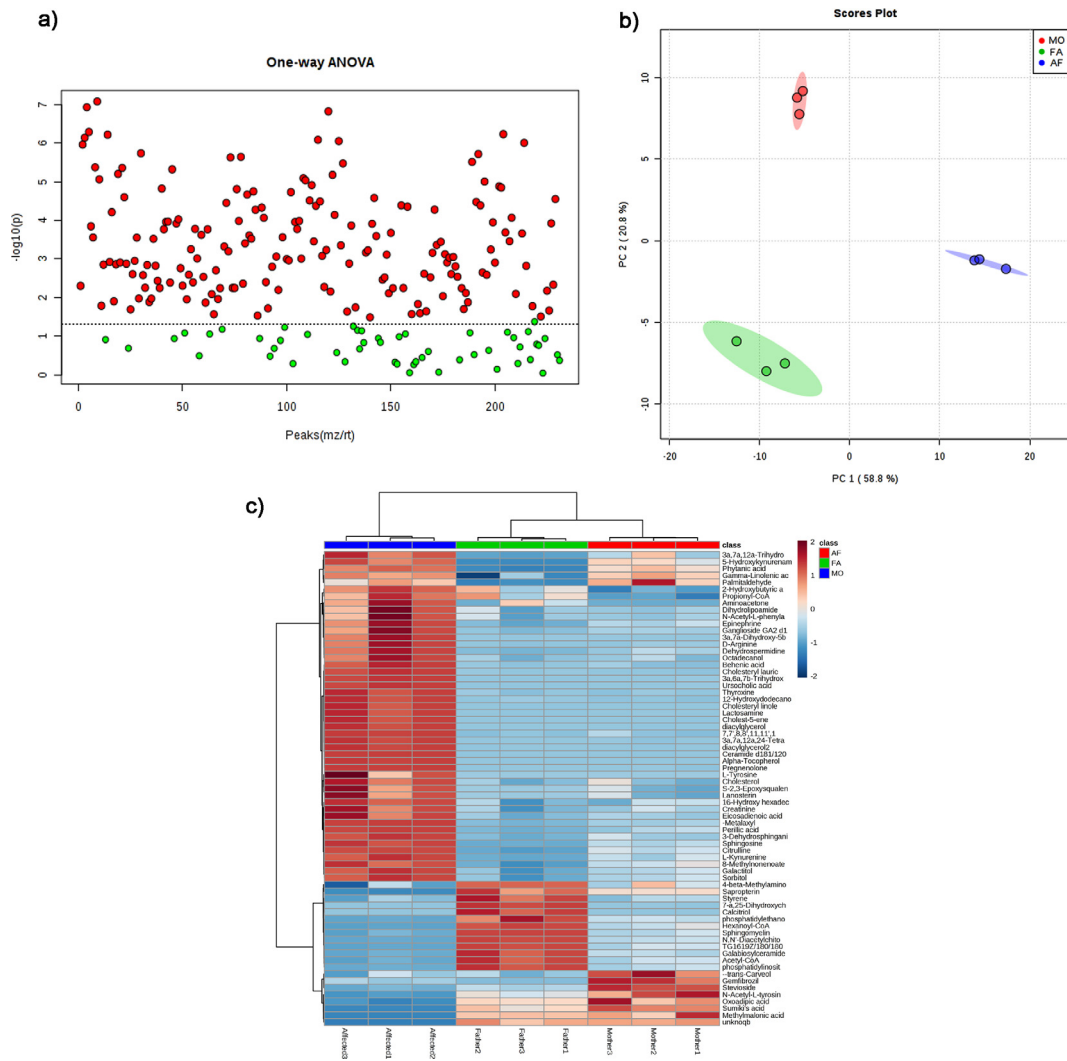
Fig. 4. (a). One-way ANOVA test illustrating the 151 significant metabolites (red circles) identified in trio. (b). PCA graphical analysis. The graph represents three clustered patterns of overlapped features among patient (red cluster), father (green cluster) and mother (blue cluster). (c). Heatmap of Metabolomics Data shows the distribution of different plasma metabolites that were significantly different between parents and CKD patient.
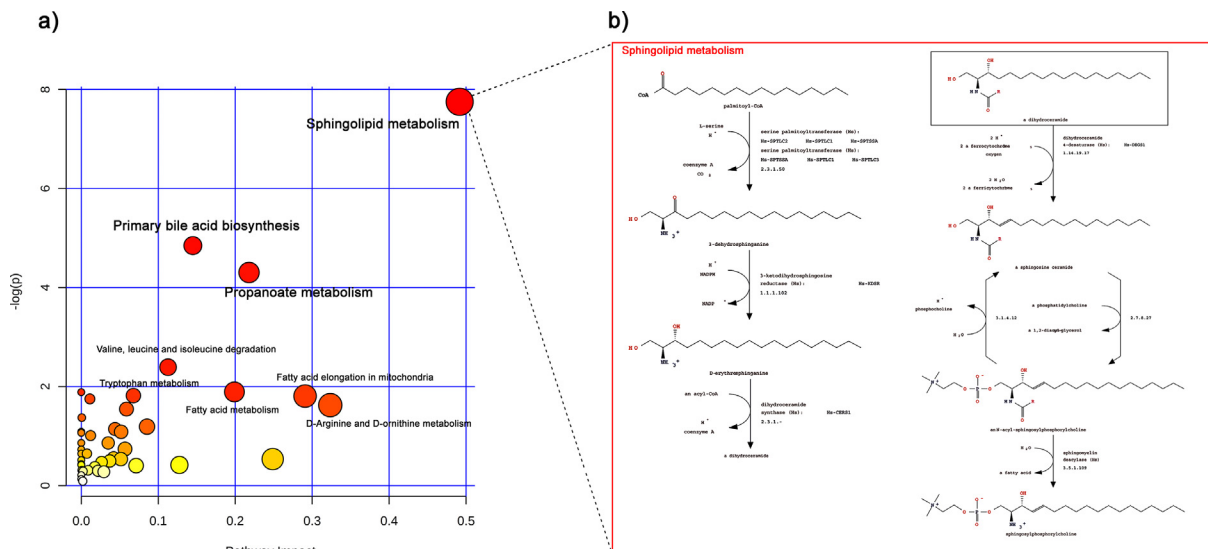

Fig. 5. Metabolic pathway impact analysis using MetaboAnalyst 3.0 program. The impact value is scaled between 0.0 and 0.5. The sphingolipid metabolites showed the highest impact value (0.5) compared to other metabolic compounds.

Table 1

Metabolic pathways enriched in the plasma sample of the CKD patient family. Subset of metabolic pathways were significantly enriched (p < 0.05). *Sphingolipid metabolism was the most significant pathway involved in the proband (p = 0.000569).

Metabolic pathway	Total	Expected	Hits	P-value	FDR	Impact
Sphingolipid metabolism*	25	0.71666	5	0.000569	0.045531	0.49166
Primary bile acid biosynthesis	47	1.3473	5	0.010081	0.40325	0.14499
Propanoate metabolism	35	1.0033	4	0.016575	0.442	0.21799
beta-Alanine metabolism	28	0.80266	3	0.04427	0.8854	0.07744
Valine, leucine and isoleucine degradation	40	1.1467	3	0.10498	1	0.11277
Synthesis and degradation of ketone bodies	6	0.172	1	0.16029	1	0
Fatty acid metabolism	50	1.4333	3	0.171	1	0.199
Fatty acid elongation in mitochondria	27	0.77399	2	0.18015	1	0.29083
Tryptophan metabolism	79	2.2646	4	0.1887	1	0.06772
D-Arginine and D-ornithine metabolism	8	0.22933	1	0.20787	1	0.32353
Lysine biosynthesis	32	0.91732	2	0.23311	1	0.05875

Table 2

The top metabolites found to be altered in plasma sample of the CKD patient (p < 0.05).

Metabolite	F value	P value	-log10(p)	FDR
Ceramide	149,030	8.16E-15	14.089	5.63E-13
Pregnenolone	14,095	9.63E-12	11.016	3.32E-10
Alpha-Tocopherol	11,197	1.92E-11	10.716	4.42E-10
3a,6a,7b-Trihydroxy-5b-cholanoic acid	3275.5	7.66E-10	9.1157	1.06E-08
Ursocholic acid	3275.5	7.66E-10	9.1157	1.06E-08
Diacylglycerol	2276.4	2.28E-09	8.6421	2.25E-08
7-a,25-Dihydroxycholesterol	2111.2	2.86E-09	8.5441	2.46E-08
Sphingosine	769.12	5.87E-08	7.2317	3.11E-07
12-Hydroxydodecanoic acid	715.31	7.28E-08	7.1376	3.59E-07
Citrulline	599.77	1.23E-07	6.9091	5.38E-07
Cholest-5-ene	597.55	1.25E-07	6.9043	5.38E-07
Thyroxine	469.58	2.56E-07	6.5921	1.04E-06
Sphingomyelin	434.4	3.23E-07	6.4913	1.24E-06
Cholesterol	28.797	0.00084	3.0758	0.001054

deformities, renal defect, neonatal hypotonia, myopathy, seizures, and early childhood deaths. Also, multiple enzymes of the mitochondrial respiratory pathway were deficient as confirmed by biochemical studies (Garcia-Diaz et al., 2012; Ng et al., 2016). The emergence of clinical symptoms suggests that causal mutations in *RMND1* gene and other genes involved in mitochondrial pathways determine the downstream clinical spectrum and affected tissues (Ng et al., 2016). In our study, we identified a very rare coding mutation in the *RMND1* gene (c.631G > A, p.(Val211Met)) in the affected proband of a consanguineous Palestinian couple segregating in an autosomal recessive inheritance mode through WES. The pathogenicity of this variant was assessed as probably damaging using *in-silico* analysis of multiple computational tools such as VEP, SIFT, PolyPhen-2, and M-CAP. The deleterious effect of the mutation was also supported by the absence of the variant in the general population asper ExAC and SHGP databases. Moreover, the clinical presentation of the mixed phenotypes in our case aligns with mitochondrial respiratory chain deficiency. This highly suggests that the *RMND1* gene have an important role in mitochondrial disease pathways involving neurological, renal, and cardiac systems.

This mutation was validated in this family using targeted sequencing of the DNA samples of the proband and parents. Parents were apparently healthy and heterozygous carriers for the identified mutation, consistent with the recessive mode of inheritance. Thus, further mutation screening is recommended for first degree relatives and distant family members to offer them better clinical management and risk assessment for successive generations. As per the previous studies (Ng et al., 2016), clinical severity caused by *RMND1* mutations is variable ranging from infantile encephalomyopathy with early childhood death to a longer survival childhood-onset nephropathy. The two first degree relatives in our studied family, were deceased in childhood (7 years),

implicating the impact of identified pathogenic variant segregating in this family. Consistent with previous findings (Gupta et al., 2016), genetic variants encompassing *RMND1* gene showed association with deafness, end stage renal failure, dilated cardiomyopathy and neurological defects underlying mitochondrial diseases. Likewise, the proband displayed neurological symptoms presented as multiple seizure attacks and renal defects (CKD stage 3), but the cardiac assessment was normal. The absence of cardiac abnormality could be explained by the difference in identified mutations between this family and previously reported cases.

It has been explained that mitochondrial metabolic defect was associated with *RMND1* mutations owing to the subsequent complexity of phenotypes. However, due to the lack of molecular functional evidence on *RMND1* mutations including its associated metabolic defects, we sought to make more in-depth pathway analysis and deduce the underlying defect of cellular metabolic network. Such analysis will help in identifying the key metabolites interacting directly or indirectly with *RMND1* protein and provide further insights about the possible metabolic role of *RMND1* towards the downstream pathology.

Metabolomic analysis in this study revealed that ceramide is one of the significantly accumulated metabolites in the patient sample. Earlier work established that ceramide belongs to sphingolipids that play an important role in regulating cellular signaling cascades. Cellular apoptosis and growth arrest is induced by ceramide metabolite (Bartke and Hannun, 2009; Hannun and Obeid, 2011). Mitochondria primarily regulate ceramide-induced apoptosis via modification of mitochondrial outer membrane permeability (MOMP) (Siskind, 2005; Colombini, 2010). Ceramide boosts oligomerization of ceramide channel, Bcl-2 pro-apoptotic proteins, and decreases anti-apoptotic proteins in the MOMP. This process changes MOMP, accompanied by the production of reactive oxygen species (ROS), release of cytochrome *C* into the cytosol, and the
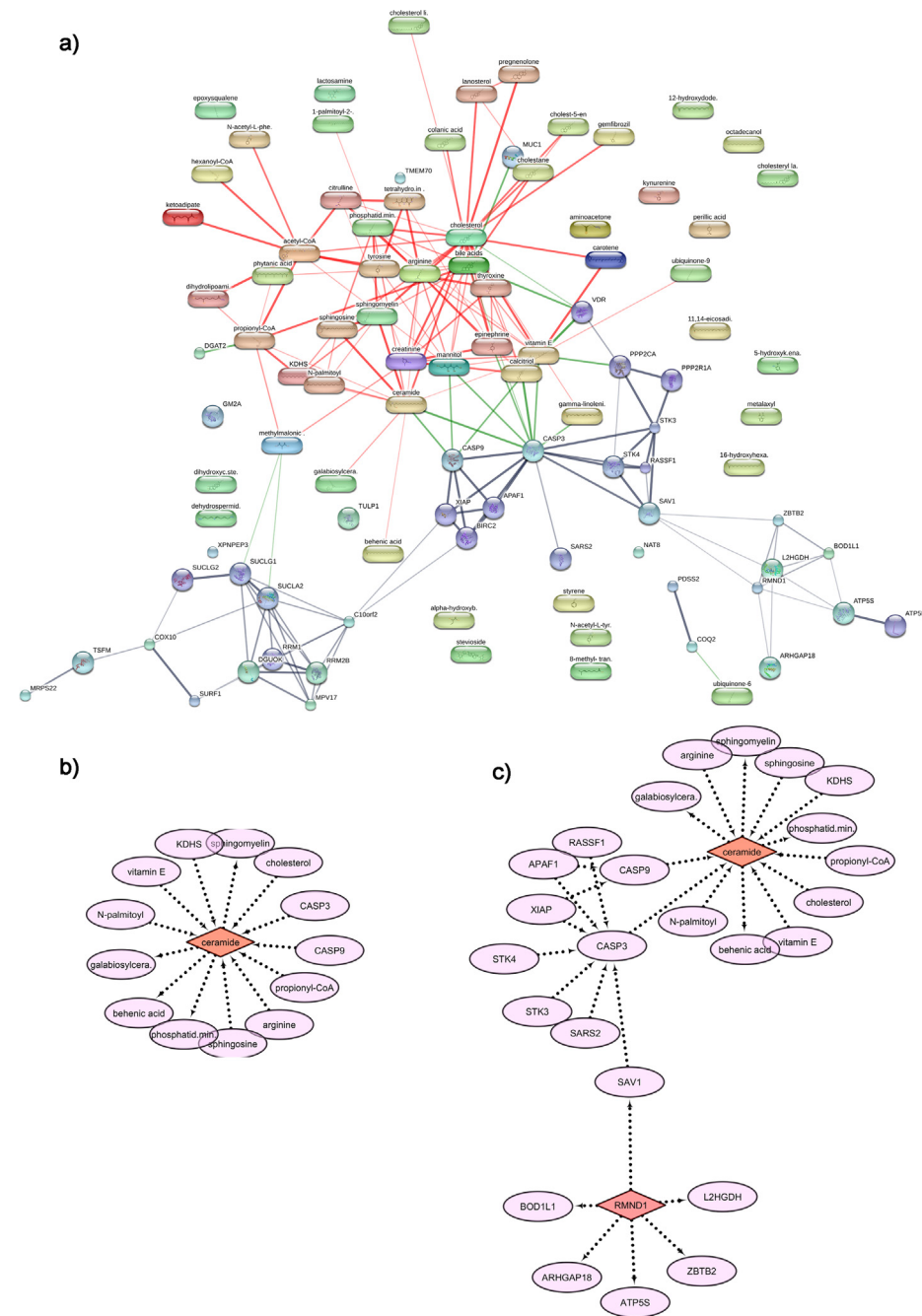
Fig. 6. Metabolite-protein interactions cluster of networks using STITTCH tools (a,b,c). The clustered metabolic network reveals the interaction between ceramide (orange diamonds) with other metabolites including lipid metabolomic compounds (a). Ceramide showed direct interactions within Caspase cascade (CASP 3 & CASP 9) (b). Ceramide showed indirect interaction with *RMND1* (red diamond) via CASP 3 (c).

start of caspase and apoptotic pathways (Siskind, 2005; Colombini, 2010). It has been demonstrated earlier that mitochondria supplies ATP, which activates caspase-9 (Nicotera and Melino, 2004). Intracellular ATP depletion in mitochondria can shift the cell death process from apoptosis to necrosis (Nicotera and Melino, 2004). The present work revealed a direct interaction between ceramide and apoptotic proteins (caspase 9 and caspase 3). Hence, it is plausible to assume that accumulated levels of ceramide in the proband was due to an underlying mitochondrial metabolic defect leading to sphingolipid apoptotic pathway deficiency and subsequent tissue damage.

We hypothesize that the mutated structure of *RMND1* had altered the synthesis of oxidative phosphorylation enzyme affecting the downstream regulation of mitochondrial metabolic network. One of the important pathways is dysregulation of sphingolipid metabolism reflected in apoptotic signaling dysregulation in the mitochondrial compartments leading to possible tissue necrosis. This highly suggests that the progression of kidney disease is mainly governed by the disturbed balance between apoptotic and antiapoptotic signaling proteins resulting in dysregulated apoptosis and subsequent glomerular cell injury. Sphingolipids and anti-apoptotic proteins play a crucial role in glomerular injury regulation and complications related to CKDs (Ueda, 2017).

In conclusion, the current work provided a novel connection between ceramide and *RMND1* through metabolomic profiling of
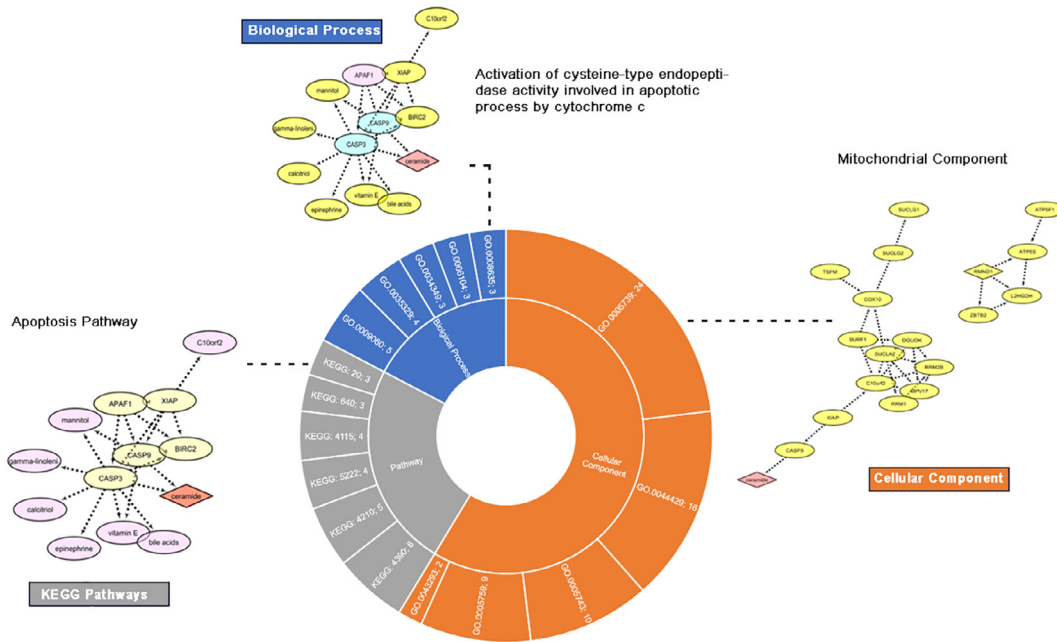
Fig. 7. Sunburst graph of ceramide and its associated genes by GO enrichment analysis (biological process, cellular component and pathways).
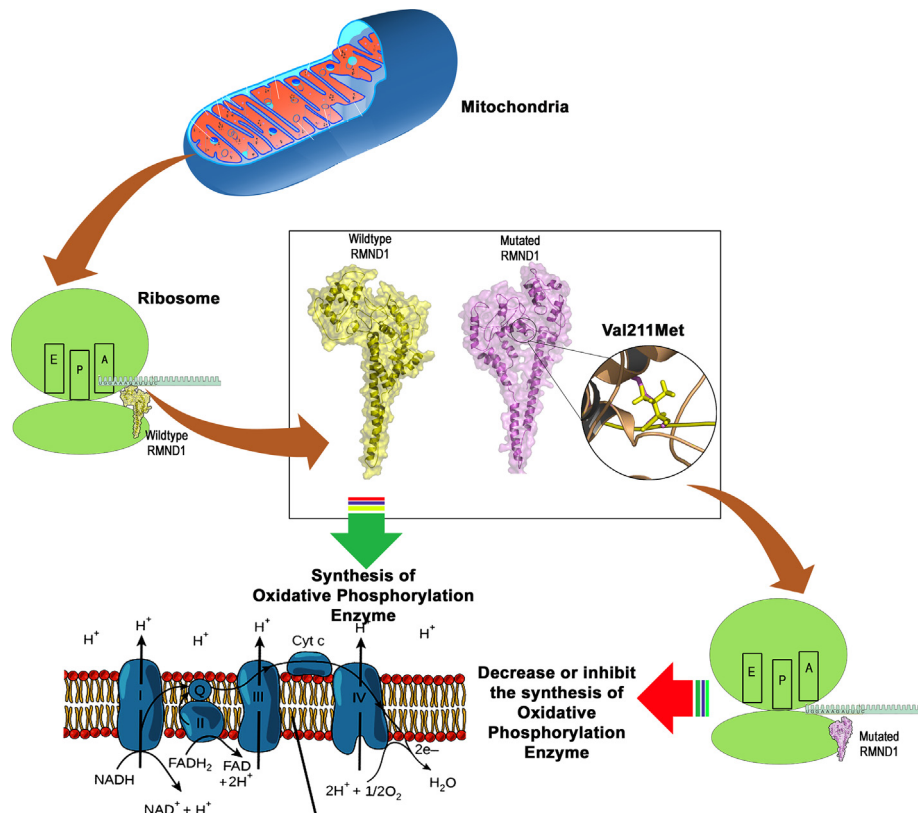

Fig. 8. Illustrated the overview of RMND1 mechanism.

a family who carries the rare mutation in the gene. This new finding demonstrated the metabolic complexity of pathological changes relating to the phenotypic spectrum. The present work provided preliminary insight into the potential role of *RMND1* protein in mitochondrial metabolic cascade and ceramide induced apoptosis defect owing to possible multi-tissue damage. Until present, no such data is demonstrating the functional link between

RMND1 and ceramide. To our knowledge, the present study is the first that showed an indirect relationship highlighting the potential role of *RMND1* on dysregulated apoptosis, leading to metabolic pathology and the complex nature of the disease. Gene expression analysis of possible upregulated and downregulated metabolites would be valuable to specifically dissect the targeted metabolomes involved, and deduce the downstream cellular regulatory path-

ways. Consequently, functional genomic analysis by generating series of knockout mice models of *RMND1* gene will provide direct evidence about the critical metabolic pathway and the panel of key metabolites directly or indirectly interacting with *RMND1* gene to better explain the complex pathology.

Acknowledgement

Author contribution statement

NG, ER and NS conceptualization and design of the study; BB, KN, HN and MR formal analysis; BB, NS and ER investigation; NS and BB methodology; BB and IK resources; NS, ER and JA supervision; BB, MA validation, NG, BB, KN, MR, MA, LA, TA, OS, JA, IK, ER and writing original draft, and writing review and editing; BB data curation, software, and visualization; NS funding acquisition and project administration.

Declaration of Competing Interest

Authors declare that there no conflicts of interests exist for this manuscript.

References

Abbiss, H., Maker, G.L., Trengove, R.D., 2019. Metabolomics approaches for the diagnosis and understanding of kidney diseases. Metabolites, 9.
Al-Aama, J.Y., Shaik, N.A., Banaganapalli, B., Salama, M.A., Rashidi, O., Sahly, A.N., Mohsen, M.O., Shawoosh, H.A., Shalabi, H.A., Edreesi, M.A., Alharthi, S.E., Wang, J., Elango, R., Saadah, O.I., 2017. Whole exome sequencing of a consanguineous family identifies the possible modifying effect of a globally rare AK5 allelic variant in celiac disease development among Saudi patients. PLoS ONE 12. e0176664.
Al-Abbasi, F.A., Mohammed, K., Sadath, S., Banaganapalli, B., Nasser, K., Shaik, N.A., 2018. Computational protein phenotype characterization of IL10RA mutations causative to early onset inflammatory bowel disease (IBD). Front. Genet. 9, 146.
Bartke, N., Hannun, Y.A., 2009. Bioactive sphingolipids: metabolism and function. J. Lipid Res. 50 (Suppl), S91–96.
Casey, J.P., Crushell, E., Thompson, K., Twomey, E., He, L., Ennis, S., Philip, R.K., Taylor, R.W., King, M.D., Lynch, S.A., 2016. Periventricular calcification, abnormal pterins and dry thickened skin: expanding the clinical spectrum of RMND1?. JIMD Rep. 26, 13–19.
Che, R., Yuan, Y., Huang, S., Zhang, A., 2014. Mitochondrial dysfunction in the pathophysiology of renal diseases. Am. J. Physiol. Renal. Physiol. 306, F367–378.
Colombini, M., 2010. Ceramide channels and their role in mitochondria-mediated apoptosis. BBA 1797, 1239–1244.
Davies, R., 2018. The metabolomic quest for a biomarker in chronic kidney disease. Clin. Kidney J. 11, 694–703.
Finsterer, J., Frank, M., 2016. Prevalence of neoplasms in definite and probable mitochondrial disorders. Mitochondrion 29, 31–34.
Finsterer, J., Scorza, F.A., 2017. Renal manifestations of primary mitochondrial disorders. Biomed. Rep. 6, 487–494.
Garcia-Diaz, B., Barros, M.H., Sanna-Cherchi, S., Emmanuele, V., Akman, H.O., Ferreiro-Barros, C.C., Horvath, R., Tadesse, S., El Gharaby, N., DiMauro, S., De Vivo, D.C., Shokr, A., Hirano, M., Quinzii, C.M., 2012. Infantile encephaloneuromyopathy and defective mitochondrial translation are due to a homozygous RMND1 mutation. Am. J. Hum. Genet. 91, 729–736.
Gupta, A., Colmenero, I., Ragge, N.K., Blakely, E.L., He, L., McFarland, R., Taylor, R.W., Vogt, J., Milford, D.V., 2016. Compound heterozygous RMND1 gene variants associated with chronic kidney disease, dilated cardiomyopathy and neurological involvement: a case report. BMC Res. Notes 9, 325.
Hannun, Y.A., Obeid, L.M., 2011. Many ceramides. J. Biol. Chem. 286, 27855–27862.
Janer, A., Antonicka, H., Lalonde, E., Nishimura, T., Sasarman, F., Brown, G.K., Brown, R.M., Majewski, J., Shoubridge, E.A., 2012. An RMND1 Mutation causes encephalopathy associated with multiple oxidative phosphorylation complex deficiencies and a mitochondrial translation defect. Am. J. Hum. Genet. 91, 737–743.
Janer, A., van Karnebeek, C.D., Sasarman, F., Antonicka, H., Al Ghamdi, M., Shyr, C., Dunbar, M., Stockler-Ispiroglu, S., Ross, C.J., Vallance, H., Dionne, J., Wasserman, W.W., Shoubridge, E.A., 2015. RMND1 deficiency associated with neonatal lactic acidosis, infantile onset renal failure, deafness, and multiorgan involvement. Eur. J. Hum. Genet. 23, 1301–1307.
Kalim, S., Rhee, E.P., 2017. An overview of renal metabolomics. Kidney Int. 91, 61–69.
Kemp, J.P., Smith, P.M., Pyle, A., Neeve, V.C., Tuppen, H.A., Schara, U., Talim, B., Topaloglu, H., Holinski-Feder, E., Abicht, A., Czermin, B., Lochmuller, H., McFarland, R., Chinnery, P.F., Chrzanowska-Lightowlers, Z.M., Lightowlers, R. N., Taylor, R.W., Horvath, R., 2011. Nuclear factors involved in mitochondrial translation cause a subgroup of combined respiratory chain deficiency. Brain 134, 183–195.
Ng, Y.S., Alston, C.L., Diodato, D., Morris, A.A., Ulrick, N., Kmoch, S., Houstek, J., Martinelli, D., Haghighi, A., Atiq, M., Gamero, M.A., Garcia-Martinez, E., Kratochvilova, H., Santra, S., Brown, R.M., Brown, G.K., Ragge, N., Monavari, A., Pysden, K., Ravn, K., Casey, J.P., Khan, A., Chakrapani, A., Vassallo, G., Simons, C., McKeever, K., O'Sullivan, S., Childs, A.M., Ostergaard, E., Vanderver, A., Goldstein, A., Vogt, J., Taylor, R.W., McFarland, R., 2016. The clinical, biochemical and genetic features associated with RMND1-related mitochondrial disease. J. Med. Genet. 53, 768–775.
Nicotera, P., Melino, G., 2004. Regulation of the apoptosis-necrosis switch. Oncogene 23, 2757–2765.
Rodrigues, C.H., Pires, D.E., Ascher, D.B., 2018. DynaMut: predicting the impact of mutations on protein conformation, flexibility and stability. Nucleic Acids Res. 46, W350–W355.
Shaik, N.A., Banaganapalli, B., 2019. Computational molecular phenotypic analysis of PTPN22 (W620R), IL6R (D358A), and TYK2 (P1104A) gene mutations of rheumatoid arthritis. Front. Genet. 10, 168.
Siskind, L.J., 2005. Mitochondrial ceramide and the induction of apoptosis. J. Bioenerg. Biomembr. 37, 143–153.
Taylor, R.W., Pyle, A., Griffin, H., Blakely, E.L., Duff, J., He, L., Smertenko, T., Alston, C. L., Neeve, V.C., Best, A., Yarham, J.W., Kirschner, J., Schara, U., Talim, B., Topaloglu, H., Baric, I., Holinski-Feder, E., Abicht, A., Czermin, B., Kleinle, S., Morris, A.A., Vassallo, G., Gorman, G.S., Ramesh, V., Turnbull, D.M., Santibanez-Koref, M., McFarland, R., Horvath, R., Chinnery, P.F., 2014. Use of whole-exome sequencing to determine the genetic basis of multiple mitochondrial respiratory chain complex deficiencies. JAMA 312, 68–77.
Ueda, N., 2017. Sphingolipids in genetic and acquired forms of chronic kidney diseases. Curr. Med. Chem. 24, 1238–1275.